AFRL-RX-WP-TM-2014-0011

ALLOYING-ELEMENT LOSS DURING HIGH-TEMPERATURE PROCESSING OF A NICKEL-BASE SUPERALLOY (PREPRINT)

S.L. Semiatin, A.L. Pilchak, and D.L. Ballard

AFRL/RXCM

JANUARY 2013
Final Report

AIR FORCE RESEARCH LABORATORY
MATERIALS AND MANUFACTURING DIRECTORATE
WRIGHT-PATTERSON AIR FORCE BASE, OH 45433-7750
AIR FORCE MATERIEL COMMAND
UNITED STATES AIR FORCE

NOTICE AND SIGNATURE PAGE

Using Government drawings, specifications, or other data included in this document for any purpose other than Government procurement does not in any way obligate the U.S. Government. The fact that the Government formulated or supplied the drawings, specifications, or other data does not license the holder or any other person or corporation; or convey any rights or permission to manufacture, use, or sell any patented invention that may relate to them.

This report was cleared for public release by the USAF 88th Air Base Wing (88 ABW) Public Affairs Office (PAO) and is available to the general public, including foreign nationals.

Copies may be obtained from the Defense Technical Information Center (DTIC) (http://www.dtic.mil).

AFRL-RX-WP-TM-2014-2011 HAS BEEN REVIEWED AND IS APPROVED FOR PUBLICATION IN ACCORDANCE WITH ASSIGNED DISTRIBUTION STATEMENT.

//Signature//

DONNA L. BALLARD, Project Engineer
Metals Branch
Structural Materials Division

//Signature//

DANIEL EVANS, Chief
Metals Branch
Structural Materials Division

//Signature//

ROBERT T. MARSHALL, Deputy Chief
Structural Materials Division
Materials & Manufacturing Directorate

This report is published in the interest of scientific and technical information exchange, and its publication does not constitute the Government's approval or disapproval of its ideas or findings.

REPORT DOCUMENTATION PAGE

Form Approved
OMB No. 0704-0188

1. REPORT DATE *(DD-MM-YY)*	2. REPORT TYPE	3. DATES COVERED *(From - To)*
January 2013	Final	01 October 2008- 31 December 2012

4. TITLE AND SUBTITLE
ALLOYING-ELEMENT LOSS DURING HIGH-TEMPERATURE PROCESSING OF A NICKEL-BASE SUPERALLOY (PREPRINT)

5a. CONTRACT NUMBER
In-House

5b. GRANT NUMBER

5c. PROGRAM ELEMENT NUMBER
62102F

6. AUTHOR(S)
(see back)

5d. PROJECT NUMBER
4347

5e. TASK NUMBER

5f. WORK UNIT NUMBER
X02R

7. PERFORMING ORGANIZATION NAME(S) AND ADDRESS(ES)
(see back)

8. PERFORMING ORGANIZATION REPORT NUMBER

9. SPONSORING/MONITORING AGENCY NAME(S) AND ADDRESS(ES)
Air Force Research Laboratory
Materials and Manufacturing Directorate
Wright-Patterson Air Force Base, OH 45433-7750
Air Force Materiel Command
United States Air Force

10. SPONSORING/MONITORING AGENCY ACRONYM(S)
AFRL/RXCM

11. SPONSORING/MONITORING AGENCY REPORT NUMBER(S)
AFRL-RX-WP-TM-2014-0011

12. DISTRIBUTION/AVAILABILITY STATEMENT
Approved for public release; distribution unlimited.

13. SUPPLEMENTARY NOTES
PA Case Number: 88ABW-2013-0096; Clearance Date: 10 Jan 2013. Journal article to be published in *Metallurgical and materials Transactions A*. This is a work of the U.S. Government and is not subject to copyright protection in the United States. Document contains color.

14. ABSTRACT (*Maximum 200 words*)
The effect of exposure at temperatures commonly used for wrought processing/heat treatment of nickel-base superalloys on the loss of alloying elements at the free surface has been determined. For this purpose, LSHR superalloy samples were exposed at 1408 K (1135°C) for 0.25 to 4 h in a vacuum or air furnace. Samples heat treated in the air furnace were either bare or enclosed in quartz capsules that had been evacuated or backfilled with argon. Following heat treatment, the alloy composition as a function of depth below the surface was determined by wavelength dispersive spectroscopy. Samples that had been heat treated in the vacuum furnace exhibited significant depletion of only chromium, a behavior explained on the basis of its high activity in nickel solid solution and corresponding rapid rate of evaporation. By contrast, samples heat treated in air exhibited an irregular scale at the surface and an underlying grain-coarsened, gamma-prime-depleted metal layer lean in aluminum, titanium, and chromium. A yet different behavior characterized primarily by aluminum loss at the surface was noted for samples that had been heat treated in evacuated or argon-backfilled capsules. These observations were interpreted in the context of a reaction between the quartz capsule and the aluminum evaporant.

15. SUBJECT TERMS
heat treatment, oxidation, evaporation, alloy loss, superalloys

16. SECURITY CLASSIFICATION OF:			17. LIMITATION OF ABSTRACT:	18. NUMBER OF PAGES	19a. NAME OF RESPONSIBLE PERSON (Monitor)
a. REPORT	b. ABSTRACT	c. THIS PAGE			Donna L. Ballard
Unclassified	Unclassified	Unclassified	SAR	46	19b. TELEPHONE NUMBER *(Include Area Code)* (937) 255-3811

REPORT DOCUMENTATION PAGE Cont'd

6. AUTHOR(S)

S.L. Semiatin, A.L. Pilchak, and D.L. Ballard - AFRL/RXCM
J.M. Shank - UES, Inc.
W.M. Saurber - University of Dayton
F. Zhang - Computherm, LLC
B. Gleeson - University of Pittsburgh

7. PERFORMING ORGANIZATION NAME(S) AND ADDRESS(ES)

Air Force Research Laboratory (AFRL/RXCM)
Materials and Manufacturing Directorate
Wright-Patterson Air Force Base, OH 45433

UES, Inc
4401 Dayton-Xenia Road
Dayton, OH 45432

Department of Mechanical and Aerospace Engineering
University of Dayton
300 College Park, Dayton, OH 45409

CompuTherm, LLC
Madison, WI 53719

Department of Mechanical Engineering and Materials Science
University of Pittsburgh
Pittsburgh, PA 15260

TABLE OF CONTENTS

LIST OF FIGURES

LIST OF TABLES

I. INTRODUCTION

Metallic sheet and foil are often used for the fabrication of honeycomb and truss-core structural products exhibiting light weight, high stiffness, and low thermal conductivity, or properties that are particularly useful in high-temperature aerospace applications. A number of approaches based on deformation or vapor processing have been applied for manufacturing such materials from a variety of alloys.

Wrought methods typically involve multiple heating and forging/rolling steps to convert ingot successively to billet, plate, sheet, and foil. Cold rolling in a four-high or cluster mill is preferable for final processing of foil materials which have a modicum of room-temperature ductility. By contrast, the wrought manufacture of foil of metals having limited cold workability must often be accomplished by (1) a series of steps comprising cold rolling with intermediate high-temperature anneals or (2) hot pack rolling [1, 2]. For foil products, which typically have thicknesses ranging from 100 to 250 μm, hot rolling and heat treatment steps must be designed carefully to ensure gage and composition uniformity. For example, at such small thicknesses, finish grinding to eliminate gage irregularities or surface contamination may be undesirable because of unacceptable losses in product yield.

Processes such as magnetron sputtering and electron-beam, physical vapor deposition (EBPVD) may provide attractive alternatives for making foil of hard-to-work alloys. These techniques offer the potential of producing net-shape, thin-gage product in a single manufacturing step. Thickness uniformity and composition control are still important considerations, however [1]. Moreover, the non-equilibrium nature of such processes may require a final high-temperature heat treatment to achieve a stable microstructure which is desirable for final service.

Nickel-base superalloys are among the materials for which there is a growing need for foil products having good creep and/or oxidation resistance at temperatures of the order of 0.5 – 0.8 of their absolute melting point. Not surprisingly, these alloys require special, high-temperature, thermomechanical processing (TMP) for making foil [2, 3]. During the hot pack rolling of an emerging class of superalloy which utilizes platinum-group metals to improve oxidation resistance, for instance, aluminum loss and the concomitant elimination of the gamma-prime pinning phase were postulated as the reason for the development of an undesirable coarse, columnar microstructure at the surface of foil that was otherwise fine-grained [3]. In related work involving thermomechanical *fatigue* of a single-crystal superalloy material, selective oxidation at the free surface led to the development of gamma-prime-depleted zones [4]. Despite these prior efforts, the precise effects of environment on the observed subsurface phenomena are relatively unexplored.

The objective of the present work was to establish the effect of environment on the mechanism and kinetics of alloying-element losses and concurrent microstructure evolution during heat treatments typical of those used for the processing of gamma-prime-strengthened, nickel-base superalloys. To this end, samples of the superalloy

LSHR were exposed in vacuum, air, or argon, and subsequent wavelength-dispersive spectroscopy was used to quantify near-surface composition profiles. Although specifically designed for service as an aero-engine disk alloy, LSHR was utilized as a model material to demonstrate the challenges associated with high temperature wrought processing of sheet and foil of the broad class of gamma-gamma prime superalloys.

II. MATERIAL AND PROCEDURES

A. *Material*

The material used in the present work was the powder-metallurgy superalloy LSHR (denoting “low solvus, high refractory”). Originally developed by NASA for high-strength, high-temperature applications such as jet engine disks, its alloy content in terms of aluminum, titanium, and chromium lent itself particularly well to the present work.

The material was received as a 230-mm-diameter billet with a measured composition in weight percent of 20.4 cobalt, 12.3 chromium, 3.5 aluminum, 3.5 titanium, 2.7 molybdenum, 4.3 tungsten, 1.5 niobium, 1.5 tantalum, 0.05 zirconium, 0.045 carbon, 0.027 boron, balance nickel. It had been produced by standard techniques starting with gas-atomized powder with a mesh size less than 400; the average powder-particle size was approximately 27 μm. Following atomization, the powder was subsolvus HIP’ed followed by hot extrusion to a 6:1 reduction. Its gamma-prime solvus temperature was 1430 K (1157°C). The microstructure of the as-received material comprised fine, equiaxed (recrystallized) gamma grains whose average size was 2-3 μm, gamma-prime [(Ni_3(Al,Ti)-base] precipitates of comparable size, and submicron carbides and borides. A fifteen-minute heat treatment at the subsolvus temperature used in the present work (i.e., 1408 K or 1135°C) resulted in a microstructure consisting of gamma grains ~5 μm in diameter, ~9 volume pct. of 1.5-μm diameter primary gamma-prime precipitates, and ~0.3 volume pct. of carbides and borides with an average diameter of ~0.3 μm (Figure 1) [5, 6].

B. *Procedures*

To establish the effect of atmosphere on alloy evaporation and/or oxidation without the possibly-confounding influence of impinging diffusion fields associated with the exposure of thin foil, *bulk* samples measuring 12.7 x 13.2 x 6.35 mm were electric-discharged machined (EDM’ed) from the as-received extrusion. Following EDM, each of the plan surfaces was low-stress ground to remove the recast layer and to minimize stored work that may affect diffusion.

The LSHR samples were heat treated for 0.25 to 4 h at 1408 K (1135°C), or conditions typical of those used for heat treatment or hot-pack rolling of superalloy sheet and foil. In commercial practice, heat treatment operations are usually done in a vacuum or inert-atmosphere furnace. Pack rolling is frequently performed using cans which are evacuated-and-sealed, sealed with a small amount of residual air, or left with a vent hole allowing ingress of air. These various environmental conditions were thus replicated in the present work by conducting experiments in a vacuum furnace or a conventional air (box) furnace.

For vacuum furnace heat treatment, each sample was placed on edge on a sheet of tantalum (thereby exposing both 12.7 x 13.2 mm surfaces). The furnace was

evacuated to 10^{-6} torr (~1.3 x 10^{-9} atmosphere) and heated at a rate of ~25 K/min (25°C/min) to peak temperature. Following the specified soak period, samples were cooled at a rate of ~25 K/min (25°C/min).

Heat treatment in the conventional air furnace was performed using samples without and with encapsulation. The former specimens were suspended from a fixture in the air furnace using nichrome wire wrapped around the 12.7 mm thick edges. Each of the encapsulated samples was placed in a quartz tube measuring 17-mm inner diameter, 19-mm outer diameter, and ~114-mm length. The capsules were either evacuated using a mechanical pump, thus producing a vacuum of approximately 8 milli-torr, or backfilled with 99.999-pct.-purity argon or air; the amount of argon or air was set at 0.21 atmospheres in order to produce a gas pressure within the capsule of one atmosphere at the heat treatment temperature. Each of the furnace heat treatments consisted of placing samples/capsules directly into the furnace, allowing 5 minutes for heat-up/temperature equilibration (per thermocouple measurements and heat-transfer calculations), and soaking for the pre-specified time. After the soak period, most of the samples were removed and water quenched to preserve the high-temperature microstructure and composition profile. In addition, selected *un-encapsulated* samples were *air cooled* following heat treatment to avoid rupture and loss of the scale layer formed during elevated-temperature exposure. One additional sample, enclosed in an evacuated capsule, was subjected to a long time heat treatment (lasting 24 h) to provide insight into alloying loss associated with possible interactions with quartz tubing.

After heat treatment, each sample was sectioned and prepared for metallography using standard procedures. Microstructure and composition profiles were determined in a Cameca SX-100 scanning-electron microscope via backscattered-electron (BSE) imaging and wavelength-dispersive spectroscopy (WDS), respectively. The interaction volume for the WDS measurements was estimated as ~ 3 μm diameter x ~3 μm depth.

At least four composition traverses (two from each plan surface) were made for each sample. The data for each sample/alloying element were then smoothed and averaged. An example is shown in Figure 2. These results show that the concentration profiles were relatively smooth in the region near the free surface at which oxidation and/or evaporation had led to depletion of gamma-prime-forming elements (i.e., Al, Ti) and hence had yielded a microstructure of gamma and very fine (<< 100 nm diameter), uniformly-dispersed, “cooling” gamma prime (i.e., gamma prime formed during water quenching). By contrast, at locations deeper into the material, the microstructure contained gamma, relatively-coarse primary gamma prime, and cooling gamma prime. This condition gave rise to oscillations in the composition profiles for alloying elements that partition between the phases (Al, Ti, Cr); the magnitude of a given oscillation depended on the relative amounts of gamma and primary gamma prime contained in the interaction volume of the electron beam at the specific location. These oscillations occurred about the average composition, and were thus eliminated by smoothing.

The bulk compositions measured by WDS tended to be slightly low (by ~0.25-0.5 wt. pct.) for aluminum and titanium and slightly high (by ~0.5 -1.5 wt. pct.) for chromium.

Because the broad features of alloy loss were of primary interest in the present work, these differences did not affect the overall interpretation of the results.

The approximate composition at the exposed (plan) surfaces was also determined via WDS using un-mounted halves of selected samples.

Because of mass-balance considerations, the observed subsurface diffusion behavior was indeed controlled/mediated by surface reactions such as evaporation and oxidation. The kinetics of these processes are discussed in the sections below.

III. RESULTS

The principal results from this work comprised metallographic observations and measurements of concentration profiles developed under the various environmental-exposure conditions.

A. *Metallographic Observations*

The heat-treatment environment was found to have a noticeable effect on the condition of the free surface, weight change, and the microstructure of the LSHR samples. For example, visual examination of the surfaces revealed that samples heat treated in vacuum were shiny and showed no evidence of discoloration or oxidation even after 4 h at 1408 K (1135°C) (Figure 3). Not surprisingly, scale was observed on the free surfaces of samples heat treated in air without encapsulation. On the other hand, encapsulated samples all showed some degree of dark discoloration but no obvious scale layer, irrespective of whether the environment within the quartz capsule had been vacuum, argon, or air.

From a quantitative standpoint, there was a measurable effect of heat-treatment environment on weight change. Specifically, there was a weight *loss* of 8 mg (relative to a nominal starting weight of ~8800 mg) for a 4-h exposure at 1408 K (1135°C) in the vacuum furnace. Unexpectedly, there was also a measurable weight loss for samples heated in air at 1408 K (1135°C) and then air cooled; this loss was 7 mg or 20 mg after 0.25 or 4 h, respectively. For samples heat treated in evacuated or argon-backfilled capsules for 4 h at 1408 K (1135°C), the weight change was relatively small (≤ 1 mg).

Approximate WDS data for the oxygen content at the free surface (in counts per second per nano-amp of beam current) gave insight into the relative degree of surface oxidation (Table I). The sample heat treated in the vacuum furnace had essentially the same oxygen level as the as-received (EDM'ed-and-low-stress-ground) sample, thus suggesting negligible oxygen pickup. By contrast, all of the samples heat treated in the air furnace with or without encapsulation appeared to have an oxygen level approximately one order of magnitude greater. Furthermore, energy-dispersive (x-ray) spectroscopy (EDS) suggested that the surface scale of the sample heat treated in air was primarily alumina with perhaps a small amount of an oxide of titanium.

The microstructures observed near the free surfaces in cross-sectioned samples also showed a noticeable dependence on heat-treatment environment. For the samples heat treated in the vacuum furnace (Figure 4), for instance, the grain size appeared almost unchanged relative to that in the as-received material (Figure 1) and in the base metal far from the surface. However, more-detailed observations revealed (1) a zone depleted in carbide and boride particles whose depth depended on heat treatment time (Figures 4a, b; Table II) and (2) a distinct layer of grains ~5-μm thick at the very surface of the sample heat treated for 4 h (Figure 4b). These grains appeared to be fine, but slightly elongated. Higher-magnification BSE micrographs (e.g., Figure 4c) revealed that they imaged darker on average than the gamma grains in the bulk material, thus suggesting composition changes that had possibly led to the formation of a layer of

single-phase gamma prime. Such an observation was complemented by yet higher-magnification micrographs (Figure 4d) which showed that the grains immediately beneath this surface layer comprised gamma with a very high content of fine gamma-prime precipitates typical of those formed during rapid cooling from temperatures close to the solvus.

Except for the presence of similar carbide/boride-depleted zones, the microstructures developed during heat treatment in air (Figure 5) were quite different from those in samples heat treated in the vacuum furnace. The principal differences consisted of the presence of a thin layer of scale and a region of gamma grains whose size exceeded that of grains in the base metal by a factor of 2-3. The extent of each of these features increased with exposure time (Table II). Additional BSE micrographs (using modified imaging conditions) revealed the nature of the scale, which appeared similar irrespective of whether samples had been air cooled or water quenched following heat treatment (Figure 6). Specifically, the scale appeared to comprise dark-imaging oxide intermixed with metal grains suggestive of the predominance of oxygen ingress and reaction along grain boundaries. In addition, the scale showed noticeable variation in thickness along the surface (as revealed in cross section, Figure 6c) and intermittent regions of what appeared to be scale loss (micrographs of the exposed plan-view surface, Figure 6e). These observations thus suggested that the measured weight loss during exposure in air was a result of partial scale spallation.

A third set of behaviors was found for samples heat treated in quartz capsules which had been either evacuated (Figure 7) or evacuated and backfilled with argon (Figure 8). In both of these cases, no scale was observed, but there was a layer of large grains at the surface and a carbide/boride-depleted zone, both of whose depth increased with heat-treatment time (Table II). Furthermore, the coarse surface grains developed during heat treatment in the evacuated capsule tended to be columnar (Figure 7), unlike the largely equiaxed surface grains developed during heat treatment in air (Figure 5) or capsules backfilled with argon (Figure 8). Such columnar grain structures are reminiscent of those produced during directional recrystallization [7]. However, the source of such a microstructural feature in the present work was likely related to the temporal evolution of concentration gradients (discussed in the next section) and the growth of a gamma-prime-depleted zone in which the grain-boundary pinning force was gradually relaxed.

B. *Concentration Profiles*

The heat-treatment environment also had a major effect on the chemical composition at and near the free surface as quantified by WDS traverses for aluminum, titanium, and chromium taken on sample cross-sections.

For samples heat treated in the vacuum furnace, chromium *depletion*, as indicated by a concentration gradient whose depth below the free surface increased with exposure time, was noted (Figure 9). The shapes of the profiles suggested the importance of diffusion. However, the temporal variation of chromium content at/near the free surface indicated the possible importance of a second mechanism such as

evaporation in controlling the loss of this alloying element. The vacuum-heat-treated samples also exhibited *higher* concentrations of aluminum and titanium near the free surface. For the sample vacuum heat treated for 1 h (Figure 9a), these changes could be explained on the basis of the chromium loss per se and simple mass balance calculations such as the following expression for aluminum:

$$C_{Al} = C_{Alo}/(1-\Delta C_{Cr}) , \quad (1)$$

in which C_{Al}, C_{Alo}, and ΔC_{Cr} denote the initial/final values of the aluminum concentration and the change in chromium concentration, respectively. For a chromium loss of 0.02, for example, Equation (1) reveals that the aluminum concentration would increase from 0.035 to approximately 0.036. However, such an explanation was insufficient to explain the surface values of aluminum and titanium for the 4-h vacuum heat treatment (Figure 9b) despite the large depression in surface chromium content for this trial. Rather, the noticeably negative concentration gradient for these two alloying elements was suggestive of "uphill" diffusion" due to local changes in chemical potential associated with the loss of chromium; this possibility is addressed in Section IV.A.

For samples heat treated in air, the WDS measurements in the metal substrate revealed noticeable concentration gradients for aluminum, titanium, and chromium (Figure 10). Similar to the chromium data in Figure 9, the profile depths increased with exposure time. However, the concentration of each of the three alloying elements at the metal-scale interface (i.e., position = 0 μm in Figure 10) varied little with time, thus suggesting that local equilibrium between the metal substrate and oxide scale had been established early in the oxidation process and subsequently maintained. In fact, the three plots for a given alloying element became nearly coincident by normalizing the ordinates by the far-field composition (to reduce scatter associated with WDS measurements) and the abscissas by the corresponding value of the square root of time (Figure 11), thus implying the importance of diffusion in the oxidation process.

Yet different sets of concentration profiles were found for samples that had been heat treated in evacuated capsules or capsules that had been evacuated and then backfilled with argon (Figures 12 and 13). In each of these cases, a surface depletion in aluminum concentration had developed; the similarity of the plots after normalization of the ordinates by the far-field composition and the abscissas by $x/\sqrt{t}$ (in which x and t denote the distance from the surface and the exposure time, respectively) also suggested diffusion-controlled behavior (Figure 14). Furthermore, concentration profiles for heat treatments using encapsulated samples showed a tendency for the surface to be enriched in titanium and depleted in chromium. The depth of the enrichment/depletion zones for these elements was comparable to the diffusion depth for aluminum.

The diffusion-limited kinetics for aluminum loss in evacuated capsules suggested by the data in Figure 12 were confirmed by observations for the supplemental 24-h heat treatment at 1408 K (1135°C). Much like the behavior for the vacuum-encapsulated samples which were exposed for 0.25 to 4 h, the corresponding concentration profiles

for this long-time heat treatment showed a marked gradient in aluminum and surface regions which were somewhat enriched in titanium and depleted in chromium (Figure 15a). Moreover, the aluminum concentration at the free surface and the normalized shape of the corresponding concentration profile for the long-time exposure was similar to those measured in the shorter-time experiments (Figure 14). Examination of the quartz capsule used in this long-time experiment also revealed that a thin residue had been deposited on its interior (Figure 15b). The composition of this residue (in atomic percent) was determined via EDS to be 38.4 aluminum, 1.3 titanium, and 60.3 oxygen; i.e., it was essentially Al_2O_3. In addition, SEM and EDS examination of the free-surface of the heat-treated sample revealed deposits, not evident in cross section, which were rich in silicon (Figure 15c).

With regard to cobalt variations, a four-hour vacuum heat treatment produced a very shallow layer in which the concentration increased rapidly from ~15 pct. at the surface to its bulk value (~20.4 pct.) at a depth of ~3 μm. This variation was consistent with the formation of a surface layer of gamma prime to a depth of ~4-5 μm (Figure 4c, d), which is discussed further in section III.A, and the equilibrium solubility of cobalt in gamma prime for LSHR. Measurable cobalt concentration gradients were not observed for samples heat treated in air or in capsules that had been evacuated or backfilled with argon.

IV. DISCUSSION

As summarized in the Results section, different types of alloying loss were evident for samples heat treated in a vacuum furnace, in an air furnace, or with encapsulation in an air furnace. Each behavior is addressed in a separate section below.

A. *Heat Treatment in a Vacuum Furnace*

Microstructure observations and concentration-profile measurements (Figures 4 and 9) indicated that the principal alloying element lost during heat treatment of LSHR samples in a vacuum furnace was chromium. The absence of an oxide layer at the surface, the retention of the fine gamma-grain microstructure (associated with gamma-prime pinning precipitates), and the *increase* in the aluminum and titanium contents at the free surface support this conclusion. Hence, the loss of chromium during vacuum heat treatment was analyzed in terms of the competition between diffusion of solute(s) to the free surface and their subsequent evaporation.

1. *Formulation of evaporation model*

The evaporation analysis comprised the solution of the one-dimensional diffusion equation for a semi-infinite domain subject to appropriate initial and boundary conditions, i.e.,

$$\partial C_i/\partial t = D\partial^2 C_i/\partial x^2 \text{ ,} \qquad (2)$$

in which C_i denotes the solute concentration (in kg of solute per m^3), t is time, x is the distance from the free surface, and D is the diffusivity (i.e., *interdiffusion* coefficient). The formulation of the diffusion equation above assumes that the diffusivity is constant, i.e., is not a function of composition. In addition, because of the small amount of gamma prime (and carbide/boride phases) at the heat treatment temperature used in the present work, diffusion was assumed to occur through a homogeneous nickel solid solution. Although such assumptions provide substantial simplification of the analysis, a more rigorous treatment would enable the interpretation of discontinuities in concentration profiles due to subsurface phase variations/phase changes, etc. [8].

The initial condition for the diffusion model assumed a uniform initial concentration C_o, i.e.,

$$C(x, t=0) = C_o \text{ .} \qquad (3)$$

The boundary condition comprised the specification of the flux of evaporant from the free surface, J_s (in kg/m^2s), as given by the Langmuir equation [9]:

$$J_s = X_i P_i^0 \gamma_i (M_i/ 2\pi R T)^{1/2} \text{ .} \qquad (4)$$

In Equation (4), X_i is the mole fraction of solute i in the alloy, P_i^0 is the vapor pressure of pure element i at (absolute) temperature T, γ_i is the activity coefficient of solute i, M_i is the molar mass of solute i (in kg/mol), and R is the gas constant. For solutes such as chromium (as well as aluminum and titanium) in LSHR, the mole fraction X_i is related to the concentration C_i to a good first approximation by the relation:

$$X_i = C_i/\rho_i \, , \tag{5}$$

in which ρ_i denotes the density of pure solute i. Thus, the flux boundary condition, Equation (4), becomes the following:

$$J_{s_i} = C_i \, (P_i^0 \, \gamma_i/\rho_i) \, (M_i/ 2\pi R \, T)^{1/2} \, . \tag{6}$$

Denoting $(P_i^0 \, \gamma_i/\rho_{Al}) \, (M_i/ 2\pi R \, T)^{1/2}$ as β_i and noting that the rate of evaporation at the free surface (Equation (4)) must be equal to the diffusive flux in the nickel matrix at this location, the following expression for the boundary condition is obtained:

$$- D \, (\partial C_i/\partial x) \, \big|_{surface} = C_i \, \beta_i \, . \tag{7}$$

Defining $h_i \equiv \beta_i/D$, the boundary condition then becomes:

$$(\partial C_i/\partial x) \, \big|_{surface} + h_i C_i = 0 \, . \tag{8}$$

The solution of the diffusion problem described by Equations (2), (3), and (8) when diffusion occurs through a *semi-infinite* matrix is found in Reference 10:

$$\frac{C(x,t)}{C(x,t=0)} = \mathrm{erf}(x/2\sqrt{Dt}) + \{[\exp(hx + h^2 Dt)] \cdot \mathrm{erfc}[\frac{x}{2\sqrt{Dt}} + h\sqrt{Dt}]\} \, , \tag{9}$$

in which *erfc* denotes the complementary error function. From Equation (9), the composition at the free surface (x=0) is the following:

$$\frac{C(x=0,t)}{C(x,t=0)} = [\exp(h^2 Dt)] \cdot [\mathrm{erfc}(h\sqrt{Dt})] \, . \tag{10}$$

It may also be readily shown that the total loss of solute due to evaporation is given by the following relation:

$$\text{Weight Loss (kg)} = (2AC_o/h) \int_0^{u_f} [u(\exp(u^2))(\mathrm{erfc}(u))du \, , \tag{11}$$

in which A denotes the total surface area of the sample, $u \equiv h\sqrt{Dt}$, and u_f is the value of u at the exposure time t*.

2. *Application of evaporation model*

Input data for the diffusion analysis (i.e., diffusion coefficients, vapor pressures, densities, molar masses) were obtained from published sources [11-14] (Table III). The thermodynamic correction factor for the diffusion coefficient of chromium in nickel solid solution was estimated to be approximately unity using the Pandat™ software and the PanNi™ database (CompuTherm LLC, Madison, WI); activity coefficients for the various solutes in LSHR were also estimated using Pandat™. As discussed below, values of D for lattice diffusion of chromium in disordered nickel solid solution other than that in Table III were also examined to interpret the effect of phase type (i.e., lattice diffusion through disordered gamma versus lattice diffusion through ordered gamma prime) and grain-size (which could lead to apparently higher diffusivity due to boundary diffusion).

Initial calculations comprised estimates of the evaporant flux at 1408 K (1135°C) from Equation (6) assuming C_i to be the nominal solute concentration in the alloy (Table III). These results indicated that the flux of chromium is two orders of magnitude greater than that of aluminum and five orders of magnitude greater than that of titanium. After accounting for the surface concentrations developed during heat treatment, the chromium evaporation rate was still predicted to be at least an order of magnitude greater than that for the other two alloying elements. These trends can be ascribed primarily to the very large activity coefficient of chromium relative to that for aluminum or titanium. Such a factor outweighs the effect of the higher vapor pressure of aluminum on the flux in comparison to that for chromium.

Model predictions for the chromium concentration profile based on Equation (9) and the material coefficients in Table III were compared to measurements for the 4-h heat treatment at 1408 K (1135°C) (Figure 16a). The comparison showed approximate agreement near the surface but not far from it. Some of the differences can be ascribed to uncertainty in the values of the diffusion coefficient for chromium in the LSHR superalloy and the possibility that this coefficient is composition/phase/grain-size dependent. Hence, a sensitivity analysis was performed in which additional model calculations were done assuming a diffusivity two or four times that in Table III. These latter predictions showed better agreement with the measurements far from the free surface.

The location-dependence of the diffusion coefficient of chromium which was required to provide an approximate fit to the measured concentration profile was likely a result of several factors. First, the evaporation of chromium led to the formation of a thin layer (~5-μm-thick) of gamma prime, an ordered solid solution which would have a lower diffusivity compared to a disordered nickel solid solution. In particular, the diffusivity of chromium in gamma prime at 1408 K (1135°C) is approximately 3×10^{-15} m^2/s [15]. On the other hand, the fine size of the gamma-prime grains would enhance solute transport via boundary diffusion [16, 17]. To match the experimental observations

at/near the surface, an enhancement of the diffusivity by a factor of approximately 3.3 would be required (i.e., D = 3.3 x 3 x 10^{-15} = 10^{-14} m^2/s). This factor is quite similar to that required to match the predictions deeper into the alloy in which diffusion occurred through an equally fine-grained, but disordered gamma solid solution; i.e., the concentration profile seemed to be fit better by D = 4 x 10^{-14} m^2/s, as noted above.

Another factor which may have affected the very near-surface chromium-concentration profile at longer times was the development of *negative* aluminum (and titanium) concentration gradients (Figure 9b). Because diffusivity cross terms such as $D_{Cr,Al}$ are positive [18], the *negative* aluminum/titanium gradients which developed at depths of several microns would have partially mitigated the diffusion of chromium to the surface.

Comparison of the measured and predicted *surface* chromium composition provided another test of the applicability of the model. The *measured* value (in terms of $C_{surface}/C_o$) was approximately 0.16. This compared favorably to a prediction of 0.20 for the value of D = 10^{-14} m^2/s, which provided a reasonable fit of the near-surface concentration profile through the layer of gamma-prime grains.

Evaporation model calculations were also performed for the development of concentration gradients of aluminum and titanium for the 4-h heat treatment at 1408 K (1135°C) by neglecting the chemical interactions likely responsible for the near-surface uphill diffusion shown in Figure 8b; these model results are shown in Figure 16b. The absence of sharp concentration gradients for both alloying elements mirrors the above conclusions based on the flux calculation in Table III.

As a second confirmation of the overall modeling approach, the weight loss associated with the evaporation of chromium during a 4-h heat treatment at 1408 K (1135°C) in the vacuum furnace was estimated from Equation (11) and the value of D in Table III (i.e., D = 10^{-14} m^2/s). This calculation yielded a predicted weight loss of 6.5 mg, which is in approximate agreement with the measurement of 8 mg. Weight losses associated with the evaporation of aluminum and carbon were estimated to be of the order of 0.5 mg, thus improving somewhat the agreement between the measurement and model prediction.

The chemical source of the near-surface, uphill diffusion of aluminum (and quite likely titanium) (Figure 9b) can be interpreted in the context of known thermodynamic interactions. Focusing on aluminum, Al and Cr have a positive chemical interaction such that the cross-term diffusion coefficient, D_{AlCr}, is positive [18]; Pandat™ calculations also revealed a noticeable positive dependence of the chemical potential of aluminum on chromium content. Thus, the combination of a positive D_{AlCr} and a positive and significant subsurface Cr gradient (Fig. 16a) can be concluded to have driven subsurface diffusion of Al in the negative direction (*i.e.*, toward the alloy surface) and hence up its own concentration gradient. Such a behavior is common in multicomponent systems [19].

Last, it may be surmised that the development of a layer depleted in carbides and borides during heat treatment in vacuum (as well as the other environments) can be ascribed to the selective loss of carbon and boron, which are fast-diffusing interstitial elements in nickel [20], and not to an abnormally-high flux of refractory/reactive elements (such as Nb, Ta, and Ti). Changes in local phase equilibria associated with the diffusion of aluminum, titanium, and chromium may also have contributed to dissolution/disappearance of the carbides and borides.

B. *Heat Treatment in Air*

The results in Figures 5, 6, 10, and 11 indicated the following: (1) Substantial diffusion of aluminum, titanium, and chromium through the metal substrate occurred during heat treatment in air; (2) the decreased levels of the gamma-prime forming elements (aluminum and titanium) near the metal surface shifted the phase equilibria such that the primary gamma prime was dissolved, thus giving rise to a coarse-grain gamma microstructure; (3) the depth of the coarse gamma grains (Figure 5, Table II) mirrored the depth of the zone depleted in aluminum and titanium for each heat treatment time (Figure 10); and (4) the measured weight *loss* suggested that portions of the scale formed during heat treatment had separated from the surface.

From a quantitative standpoint, the depth of the gamma-prime-depleted zone corresponded approximately to the location at which the aluminum and titanium contents had each dropped to a concentration of 3 weight percent, or 9/10 of the levels in the bulk material. For such a composition change, the solvus temperature was estimated from Pandat™ to be 1129°C, a value close to the heat-treatment temperature.

The similarity of the concentration profiles when the abscissas were normalized by the square root of time (Figure 11) suggested that solute transport through the nickel solid solution was diffusion-controlled for each alloying element. Furthermore, the concentration profiles for the three different elements each showed a similar penetration depth for a given heat treatment time, thus suggesting similar *engineering* diffusivities. An estimate of the pertinent diffusivity was obtained using the 1-D diffusion equation again (Equation (2)) with the initial condition being Equation (3). Per Figures 10 and 11, the boundary condition appeared to be that the concentration at the metal-scale surface interface was constant, i.e., C_s. The solution for this problem, assuming a stationary alloy/scale boundary as a reasonable approximation [21], is the following:

$$\frac{C(x,t) - C_S}{C_o - C_S} = \mathrm{erf}(x/2\sqrt{Dt}) \ . \qquad (12)$$

Taking $D = 4 \times 10^{-14}$ m^2/s, the solution (Equation (12)) showed relatively good agreement with the measurements summarized in Figure 10. As noted above, diffusivity cross terms (such as $D_{Al,Cr}$ and $D_{Cr,Al}$) are positive [18]. Because the aluminum, titanium, and chromium concentration gradients are all positive, the fitted value of D thus incorporates the influence of diagonal *and* off-diagonal diffusion coefficients.

Because samples heat treated in air had shown a weight *loss* (rather than a weight gain due to reaction with oxygen) and an irregular layer of scale, the net fluxes associated with the concentration profiles for aluminum, titanium, and chromium were determined. Specifically, the net flux at the free surface J_s (in kg/m^2) was determined from by the following expression derived from Equation (12):

$$J_S = -D \int_0^t \frac{\partial C}{\partial x}\Big|_s dt = -D (C_o - C_s) \int_0^t \frac{dt}{\sqrt{\pi D t}} = -[\,2 (C_o - C_s) \sqrt{D/\pi}\,]\,\sqrt{t}\ . \qquad (13)$$

Taking C_s to be 120, 120, and 720 kg/m^3 (i.e., 1.5, 1.5, and 9 w/o), the predicted weight change (= net flux x surface area) for the samples exposed in air for 4h was estimated to be 2.7, 2.7, and 6.2 mg for aluminum, titanium, and chromium, respectively. The total weight loss (2.7 + 2.7 + 6.2 = 11.6 mg) was less than the measured value of ~20 mg for this heat treatment time, however. Hence, it may be surmised that some of the oxide/base metal was lost from the surface due to the intergranular nature of the oxidation process (Figure 6d). In this regard, a 20-mg decrease in weight would correspond to merely a 3.7-μm-thick layer of metal loss if it were uniformly distributed around the sample surface. The non-uniform thickness of the scale and the somewhat rough, scalloped surface topography of the samples heat treated in air (Figure 6), which contrasts with the very smooth surfaces for samples heat treated in the vacuum furnace or in capsules in the air furnace (Figures 4, 7, 8), suggested, however, that occluded gamma grains and intergranular layers of oxide were lost due to partial scale spallation during cooling following heat treatment at 1408 K (1135°C).

It may also be hypothesized that the chromium loss during heat treatment in air may have been exacerbated by volatilization. Estimates based on the work of Stearns, *et al.* [22] suggest however that such a loss would have been small, particularly in view of the possibly viscous nature of the gas and departures from ideality.

C. *Heat Treatment in Evacuated or Argon-Backfilled Capsules*

LSHR samples heat treated in quartz capsules which were evacuated or evacuated and backfilled with argon exhibited (1) a scale-free, but discolored (and silicon-contaminated) free surface and (2) a gamma-prime depleted, coarse-grain microstructure and noticeable loss of solely aluminum near the surface. Similar to the samples heat treated in an air environment, the depth of the coarsened microstructure correlated with the penetration depth of the aluminum concentration profile.

The absence of scale of a measurable thickness for encapsulated samples can be rationalized assuming that all of the oxygen within a given capsule combined with aluminum, titanium, or chromium. Neglecting initially the possible decomposition of silica comprising the quartz capsule, in the worst case scenario (i.e., a capsule backfilled with 0.211 atm of air), there would have been 1.46 mg of oxygen within the capsule, resulting in an oxide volume of approximately 8 x 10^{-14} m^3 , irrespective of whether it was alumina, rutile, or chromia. For samples of the size used in the present work, the thickness of a uniform layer of scale with this volume would be approximately

1 μm. For the evacuated capsules or those backfilled with high-purity argon, similar calculations revealed that the oxide layer would be approximately four orders of magnitude thinner, i.e., in the range of angstroms.

The small volume of the heat-treatment capsule was concluded to be a major factor in the absence of concentration gradients for titanium and chromium. In particular, the mass flux and time required to achieve the equilibrium vapor pressure P* for each alloying element was estimated based on (1) its nominal (bulk) composition/activity coefficient, (2) Raoult's Law ($P^* = \gamma_i X_i P_i^o$), (3) the ideal gas law ($P^*V^* = nRT$, in which V^* denotes the volume of the capsule, and n is the number of moles of gas), (4) the Langmuir equation, and (5) the surface area of the sample. These estimates (Table IV) showed that the evaporant flux was quite small and the equilibrium vapor (partial) pressure for both chromium and titanium was achieved in much less than 1 s at 1408 K (1135°C).

For aluminum, the time to achieve the equilibrium vapor pressure was also predicted to be very short, i.e., << 1 s. From a thermodynamic viewpoint, however, Ellingham diagrams revealed that alumina has a considerably lower free energy than silica (quartz) [23]. By contrast, the free energies of formation of rutile or chromia are either comparable to or much greater than that of silica, respectively. Hence, it may be hypothesized that aluminum vapor in the capsule reacted with the silica to form alumina. This conclusion was supported by the observation of an alumina deposit on the inner diameter of an evacuated quartz capsule which had been used to heat treat an LSHR sample for 24 h at 1408 K (1135°C) (Figure 15b). However, it is unclear whether such a reaction was the source of the silicon found on the surface of heat treated samples themselves (Figure 15c) or whether silica from the quartz tube had evaporated and/or decomposed and then reacted with the sample surface. Similar phenomena have been observed before [24], but warrant further research.

The similarity of the aluminum concentration at the surface of samples heat treated for 0.25, 1, 4, or 24 h (Figures 12 and 15a) suggested that equilibrium between the metal surface composition, the vapor phase, and the quartz capsule was achieved early in the heat treatment. As revealed by the similar normalized concentration profiles for aluminum (Figure 14), evaporation of aluminum (and the formation of alumina) would have occurred at a decreasing rate with time due to the decreasing concentration gradient at the free surface. Furthermore, the limited/mild titanium and chromium concentration gradients developed in the evacuated-capsule heat treatments indicates that the cross effects of these elements on the diffusion of Al to the surface was relatively small.

The present results and interpretation suggest the possible efficacy of reducing/eliminating aluminum loss by use of alumina, rather than quartz, capsules. For other heat-treatment environments (e.g., vacuum and air), however, it appears that limiting the processing time and temperature is the only viable means of minimizing the loss of alloying elements at the surface. Alternatives based on alloy modification may provide another approach. In this regard, it has been noted previously [3] that the

addition of even platinum-group-metal (PGM) alloying elements, commonly used for environmental protection in service, does not prevent surface reactions under processing conditions similar to those reported herein for LSHR. By contrast, non-wrought-processing approaches, such as those based on vapor processes [25], have been proposed as means to make foil products and may enable the avoidance of detrimental high-temperature exposure of the type investigated in the present work.

V. SUMMARY AND CONCLUSIONS

Samples of the nickel-base superalloy LSHR were heat treated at 1408 K (1135°C) in a vacuum furnace, in an air furnace, or in quartz capsules that were evacuated or backfilled with argon to establish the alloying losses at the free surface. The following conclusions were drawn from this work:

1. Exposure in a vacuum furnace results primarily in the evaporation of chromium due to its high activity coefficient relative to those of aluminum and titanium. The chromium loss, coupled with enrichment in aluminum and titanium, leads to the development of a surface layer of fine gamma-prime grains and the preservation of a fine gamma grain structure beneath this layer. The development of such a surface microstructure via vacuum heat treatment can serve as the basis for the formation of oxidation-resistant, in-situ coatings.

2. Exposure in air leads to the formation of an oxide-metal scale and substantial losses of aluminum, titanium, and chromium to similar depths, thus suggesting comparable diffusivities for these three alloying elements. The loss of aluminum and titanium results in the development of a surface layer in the metal which is depleted of the gamma-prime pinning phase and hence gamma grains which are much coarser than in the bulk of the material.

3. Exposure in laboratory-scale, quartz (silica) capsules which are evacuated or backfilled with high-purity argon leads to rapid equilibration of the vapor pressures of aluminum, titanium, and chromium. The much lower free energy of alumina relative to silica appears to result in a reaction between the aluminum vapor and the capsule and hence the development of substantial aluminum loss at the surface of superalloy samples.

4. A layer depleted in carbide/boride particles is developed during heat treatment irrespective of the heat-treatment environment. The depth of this layer mirrors that of the zone depleted in the aluminum, titanium, and/or chromium.

Acknowledgements – This work was conducted as part of the in-house research of the Metals Branch of the Air Force Research Laboratory's Materials and Manufacturing Directorate. The support and encouragement of the Laboratory management and the Air Force Office of Scientific Research (Drs. A. Sayir and J. Fuller, program managers) are gratefully acknowledged. Technical discussions with T.P. Gabb and C.K Sudbrack (NASA Glenn Research Center) are gratefully acknowledged. The assistance of T.M. Brown, R.E. Turner, and F. Meisenkothen in conducting the heat treatment experiments and determining the composition of deposits on quartz capsules is appreciated. Three of the authors were supported under the auspices of contracts FA8650-08-D-5200 (JMS) FA8650-09-2-5800 (WMS), and FA8650-07-D-5800 (ALP).

REFERENCES

1. S.L. Semiatin, M.E. Gross, D.W. Matson, W.D. Bennett, C.C. Bonham, A.I. Ustinov, and D.L. Ballard: *Metall. Mater. Trans. A*, 2012, vol. 43A, in press.

2. A.L. Pilchak, D.L. Ballard, D.S. Weaver, and S.L. Semiatin: *Metall. Mater. Trans. A*, vol. 42A, 2011, pp. 1089-1102.

3. D.L. Ballard, D.S. Weaver, A.L. Pilchak, and S.L. Semiatin: *J. European Ceramic Society*, 2010, vol. 30, pp. 2305-2312.

4. J.J. Moverare and S. Johansson: *Mater. Sci. Eng. A*, 2010, vol. A527, pp. 553-558.

5. S.L. Semiatin, K.E. McClary, A.D. Rollett, C.G. Roberts, E.J. Payton, F. Zhang, and T.P. Gabb: *Metall. and Mater. Trans. A*, 2012, vol. 43A, pp. 1649-1661.

6. S.L. Semiatin, K.E. McClary, A.D. Rollett, C.G. Roberts, E.J. Payton, F. Zhang, and T.P. Gabb: submitted to *Metall. and Mater. Trans. A*, 2012.

7. J. Li, S.L. Johns, B.M. Iliescu, H.J. Frost, and I. Baker: *Acta Mater.*, 2002, vol. 50, pp. 4491-4497.

8. D.Y. Young and B. Gleeson: *Corrosion Sci.*, 2002, vol. 44, pp. 345-357.

9. I. Langmuir: *Phys. Rev.*, 1913, vol. 5, pp. 329-342

10. H.S. Carslaw and J.C. Jaeger: *Conduction of Heat in Solids*, Oxford University Press, London, 1959.

11. M.S.A. Karunaratne, D.C. Cix, P. Carter, and R.C. Reed: in *Superalloys 2000*, T.M. Pollock, R.D. Kissinger, R.R. Bowman, K.A. Green, M. McLean, S. Olson, and J.J. Schirra, eds., TMS, Warrendale, PA, 2000, pp. 263-272.

12. D.D. Pruthi, M.S. Anand, and R.P. Agarwala: *J. Nuclear Materials*, 1977, vol. 64, pp. 206-210.

13. R. Speiser, H.L. Johnston, and P. Blackburn: *J. Amer. Chem. Soc.*, 1950, vol. 72, pp. 4142-4143.

14. D.R. Lide: *CRC Handbook of Chemistry and Physics, 84th Edition*, CRC Press, Boca Raton, FL, 2003, Section 4, Properties of the Elements and Inorganic Compounds; Vapor Pressure of the Metallic Elements.

15. Y. Minamino, S.B. Jung, T. Yamane, K. Hirao: *Metall. Trans. A*, 1992, vol. 23A, pp. 2783-2790.

16. Y. Mishin and C. Herzig, : *Mater. Sci. Eng. A*, 1999, vol. A260, pp. 55-71.

17. R. Dohmen and R. Milke: *Reviews in Mineralogy & Geochemistry*, 2010, vol. 72 pp. 921-970.

18. J.W. Nesbitt and R.W. Heckel: *Metall. Trans. A*, 1987, vol. 18A, pp. 2061-2073.

19. M.A. Dayananda: *Mater. Sci. Eng. A*, 1989, vol. A121, pp. 351-359.

20. D.S. Berry: *J. Appl. Phys.*, 1973, vol. 44, pp. 3792-3793.

21. B.D. Bastow, D.P. Whittle, and G.C. Wood: *Oxidation of Metals*, 1978, vol. 12, pp. 413-438.

22. C.A. Stearns, F.J. Kohl, and G.C. Fryburg: *J. Electrochem. Soc.*, 1974, vol. 121, pp. 945-951.

23. B. Gleeson: in *Schreir's Corrosion, Volume 1*, A.J. Richardson, ed., Elsevier, Amsterdam, 2010, pp. 180-194.

24. P.Y. Hou and J. Stringer: Oxidation of Metals, 1990, vol. 33, pp. 357-369.

25. S.L. Semiatin, M.E. Gross, D.W. Matson, W.D. Bennett, C.C. Bonham, A.I. Ustinov, and D.L. Ballard, *Metall. and Mater. Trans. A*, 2012, vol. 43A, pp. 4819-4834.

Table I. Approximate Relative Oxygen Content on Free Surface of LSHR Samples Heat Treated at 1408 K (1135°C)

Atmosphere	Exposure Time (h)	Oxygen (cps/na)*
None (As Rec'd)	---	1.15
Vac Furn	4	1.30
Air (AC)	1	23.7
Air (WQ)	0.25	17.3
Air (WQ)	4	18.8
Evac caps	0.25	15.6
Evac caps	4	19.2
Air caps	0.25	12.3
Argon caps	0.25	11.6
Argon caps	4	15.2

* cps/na = counts per second per nano-amp of beam current;
AC = air cooled, WQ = water quenched

Table II. Metallographic Observations for LSHR Samples Heat Treated at 1408 K (1135°C)

Atmosphere	Exposure Time (h)	Scale Thick (μm)	Big Grains Layer (μm)	Carbide-Free Layer (μm)
Vac Furn	1	---	---	11
Vac Furn	4	---	---	67
Air	0.25	4.5	13.5	---
Air	1	5.5	30	---
Air	4	7	44.5	55
Evac Caps	0.25	---	9	17
Evac Caps	1	---	16	25
Evac Caps	4	---	41	62
Argon Caps	0.25	---	0	6
Argon Caps	1	---	17	16
Argon Caps	4	---	39	44

Table III. Input Data for Evaporation Calculations at 1408 K (1135°C)

Solute:	**Cr**	**Al**	**Ti**
D (m^2/s)	10^{-14}	$3.7x10^{-14}$	$2 x 10^{-14}$
P^o (Pa)	0.0076	0.260	0.0001
ρ (kg/m^3)	7150	2700	4505
M (kg/mol)	0.052	0.027	0.0479
γ	2.44	0.0008	0.007
C (kg/m^3)*	980	280	280
J (kg/m^2s)**	$2.1x 10^{-6}$	$1.3x10^{-8}$	$3.5x10^{-11}$

* Solute content based on nominal alloy composition and alloy density of 8000 kg/m^3.

** Flux, J, based on Equation (6).

Table IV. Estimates of the Time Required to Achieve the Equilibrium Vapor Pressure for Encapsulated LSHR Samples

Solute:	**Cr**	**Al**	**Ti**
P^o (Pa)	0.0076	0.260	0.0001
γ	2.44	0.0008	0.007
X	0.137	0.075	0.042
Evap for Equil Vapor Pressure (kg)	$2.9x10^{-13}$	$9.3x10^{-16}$	$3.2x10^{-18}$
$[C_i P_i^0 \gamma_i/\rho_i] (M_i/ 2\pi R T)^{1/2}$ (kg/m^2s)	$2.1x10^{-6}$	$1.3x10^{-8}$	$3.5x10^{-11}$
Time for Equil (s)	0.0002	0.0001	0.0001

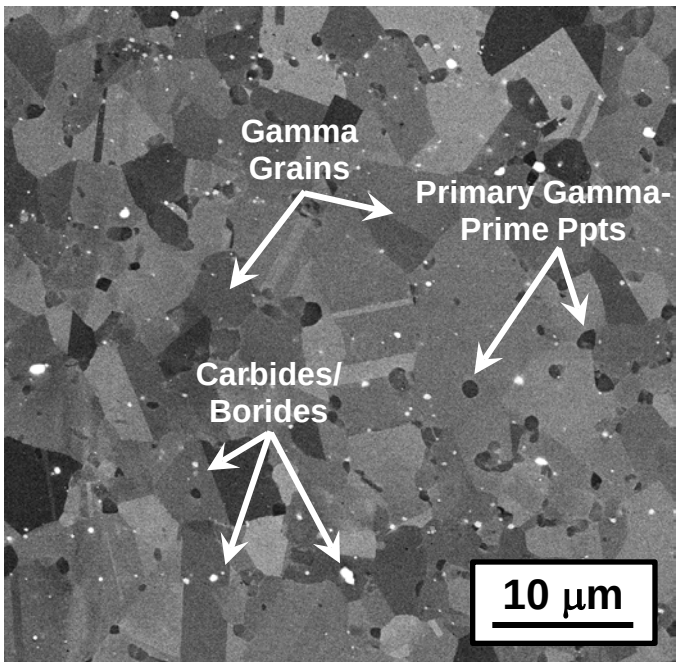

Figure 1. Backscattered electron micrograph of LSHR program material that was water quenched following a 15-minute heat treatment at 1408 K (1135°C). The coarse, equiaxed grains are gamma, the medium-size black particles are primary gamma-prime precipitates, and the fine white/gray particles are carbides and borides.

(a)

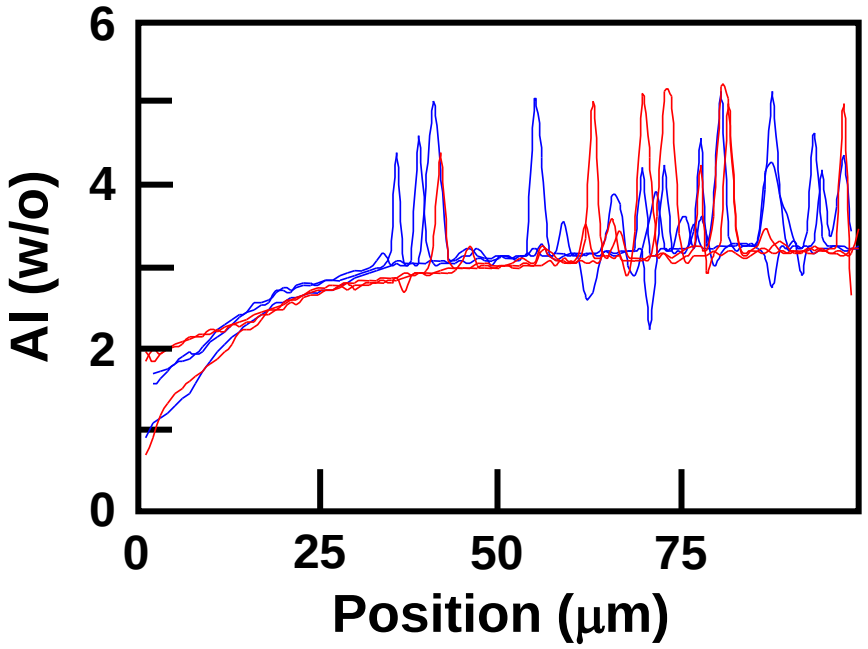

(b)

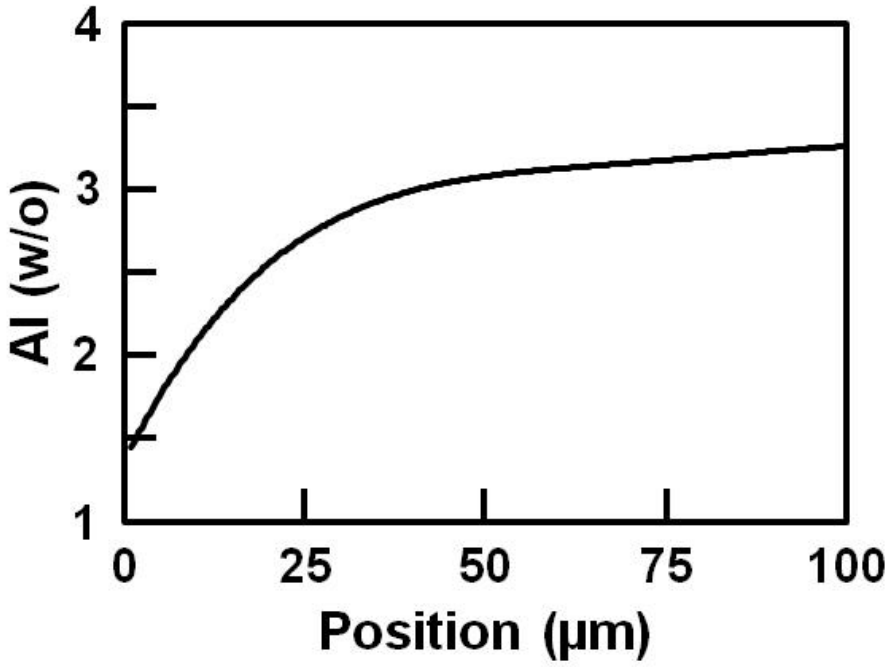

Figure 2. Aluminum concentration profiles as a function of distance from the free surface for an LSHR sample heat treated in air for 4 h at 1408 K (1135°C) and water quenched: (a) Original measurements and (b) corresponding data that have been smoothed and averaged.

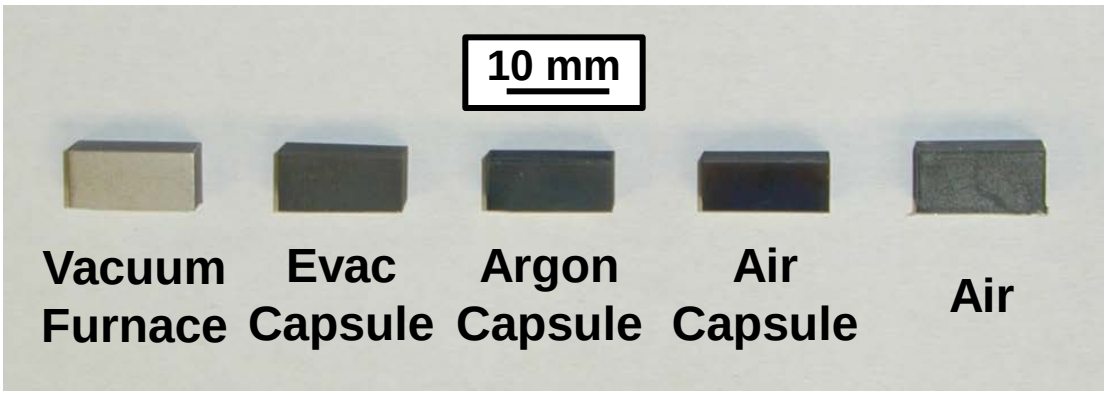

Figure 3. Macrograph of LSHR samples heat treated for 4 h at 1408 K (1135°C) in a vacuum furnace or in an air furnace with or without encapsulation as indicated.

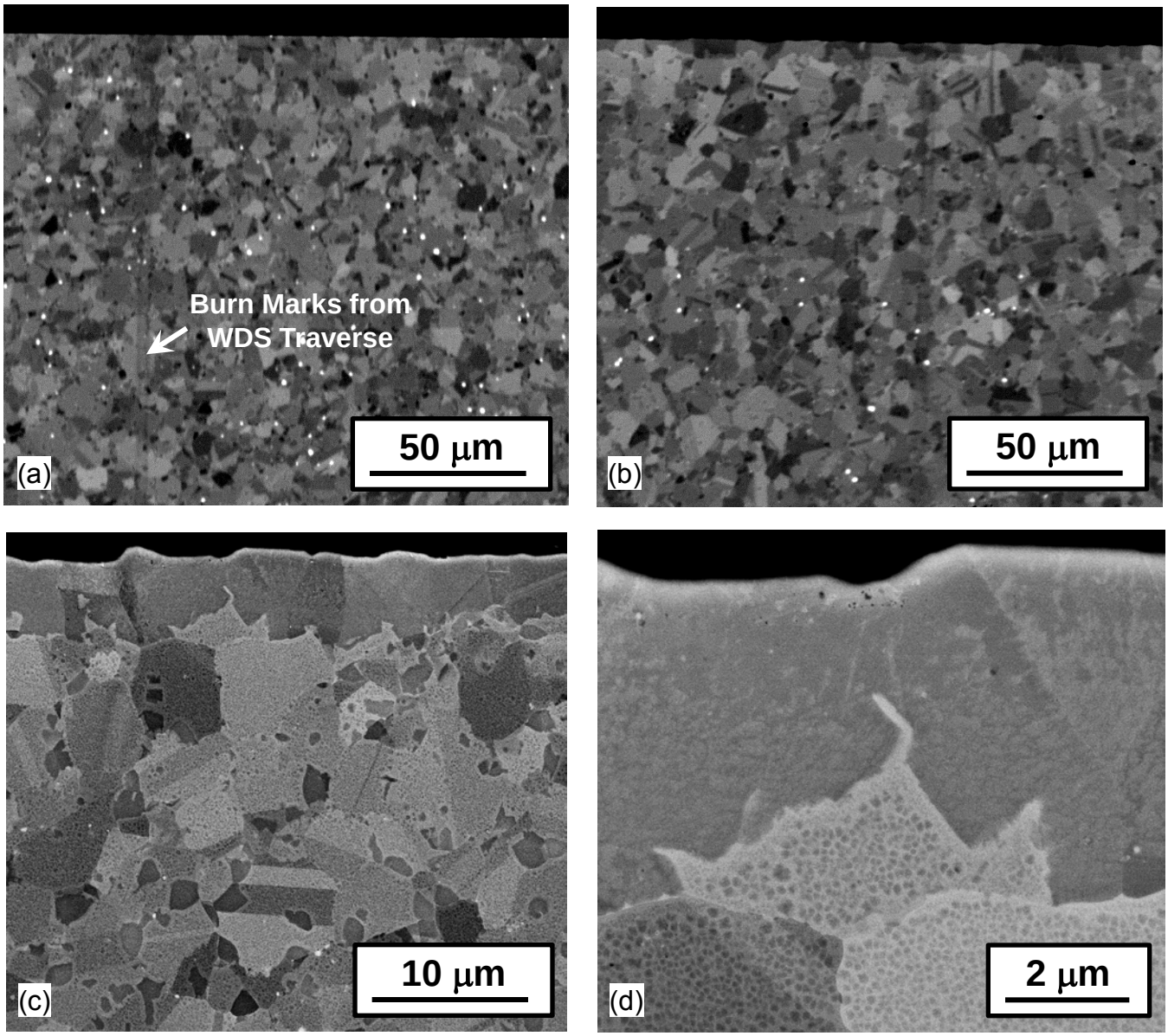

Figure 4. Micrographs of sectioned LSHR samples which were heat treated in a vacuum furnace at 1408 K (1135°C) for (a) 1 h or (b, c, d) 4h. The fine lines normal to the surface in (a) (and other micrographs) are the residue (”burn marks”) associated with WDS composition traverses.

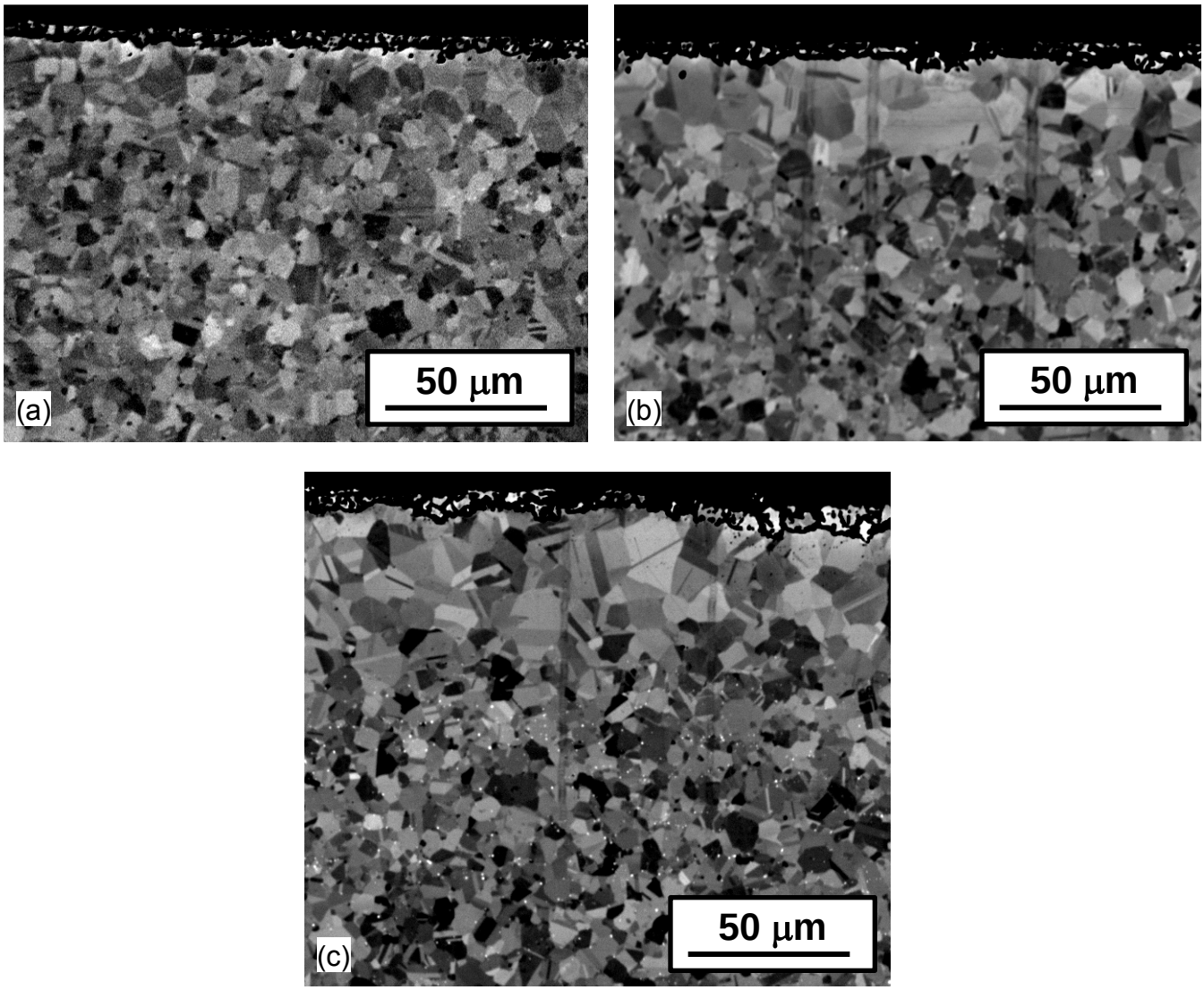

Figure 5. Micrographs of sectioned LSHR samples which were heat treated without encapsulation in an air furnace at 1408 K (1135°C) for (a) 0.25 h, (b) 1 h, or (c) 4h.

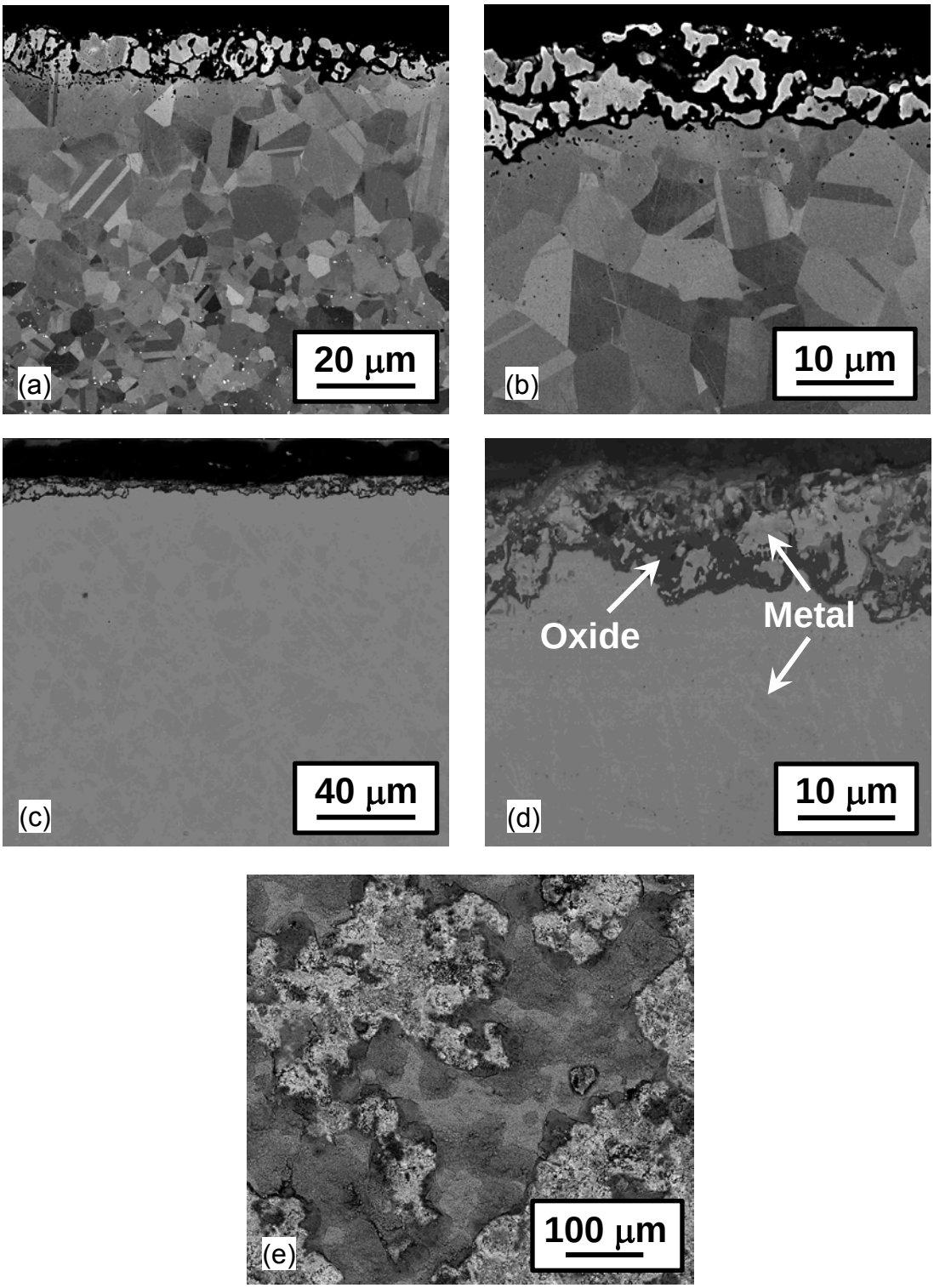

Figure 6. Micrographs illustrating the surface scale on LSHR samples which were heat treated without encapsulation in an air furnace at 1408 K (1135°C) for 4 h followed by (a, b) water quenching or (c, d, e) air cooling. The micrographs were taken from (a-d) sample cross sections or (e) the plan-view (free) surface.

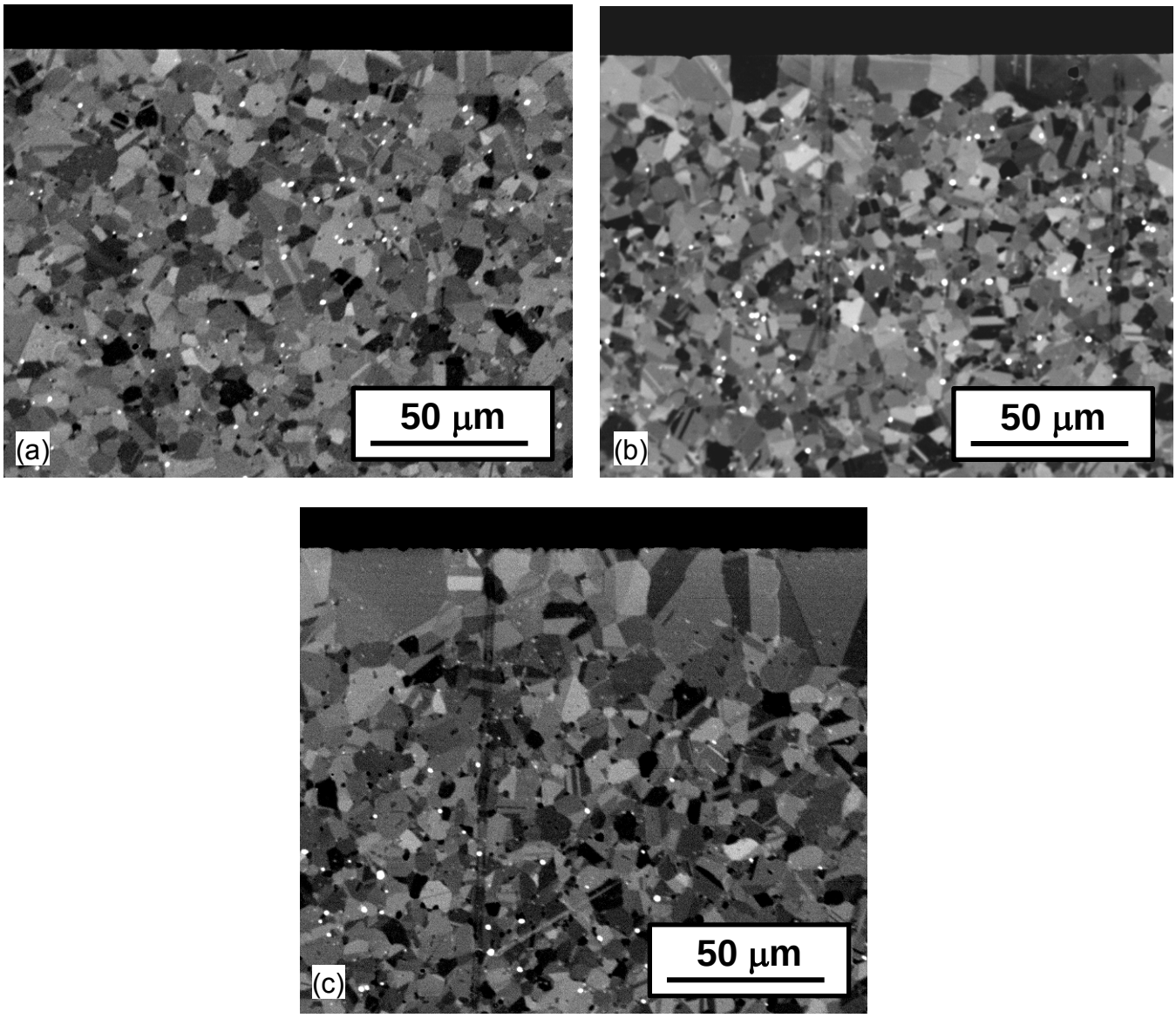

Figure 7. Micrographs of sectioned LSHR samples which were heat treated in evacuated quartz capsules in an air furnace at 1408 K (1135°C) for (a) 0.25 h, (b) 1 h, or (c) 4h.

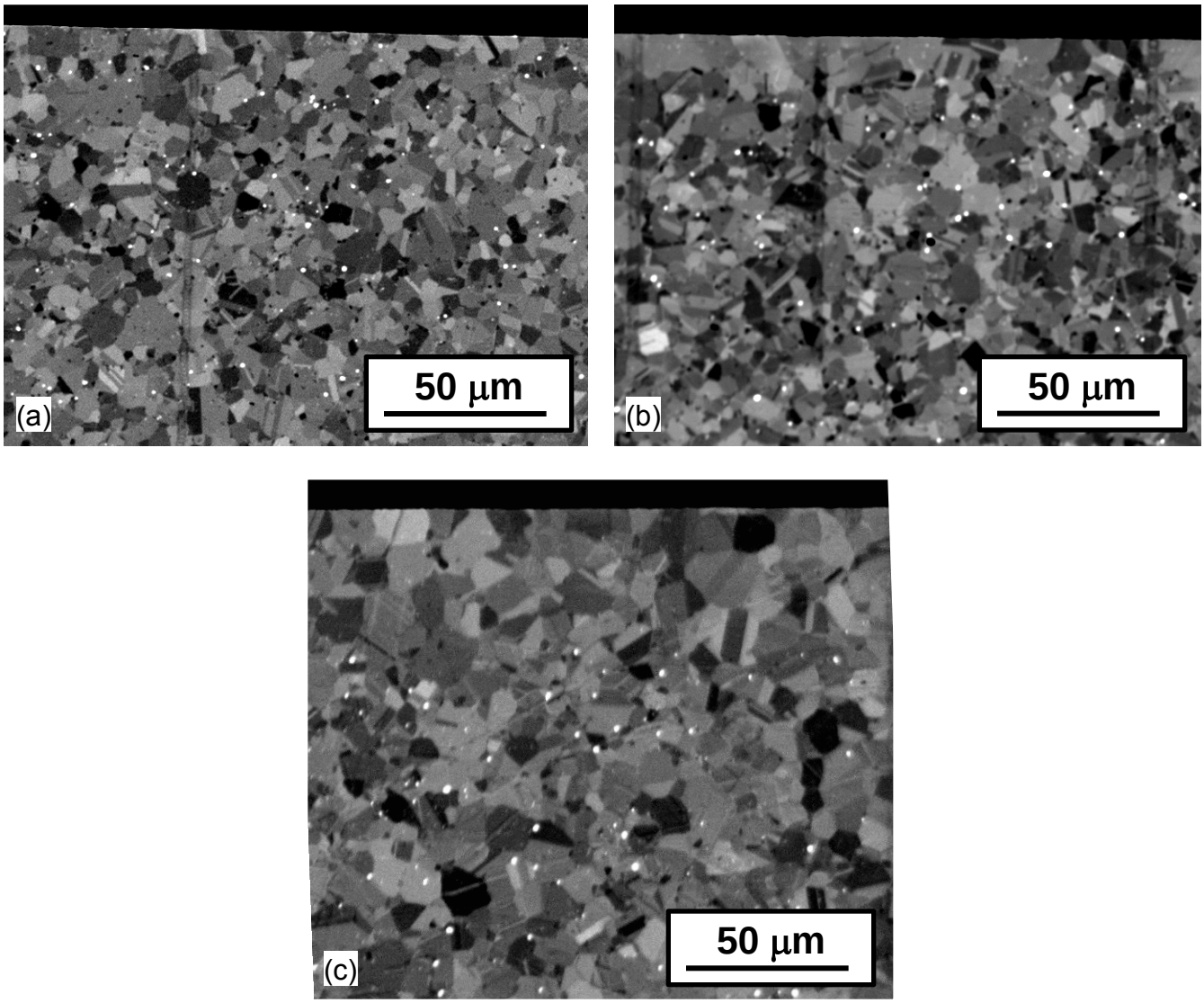

Figure 8. Micrographs of sectioned LSHR samples which were heat treated in quartz capsules backfilled with argon in an air furnace at 1408 K (1135°C) for (a) 0.25 h, (b) 1 h, or (c) 4h.

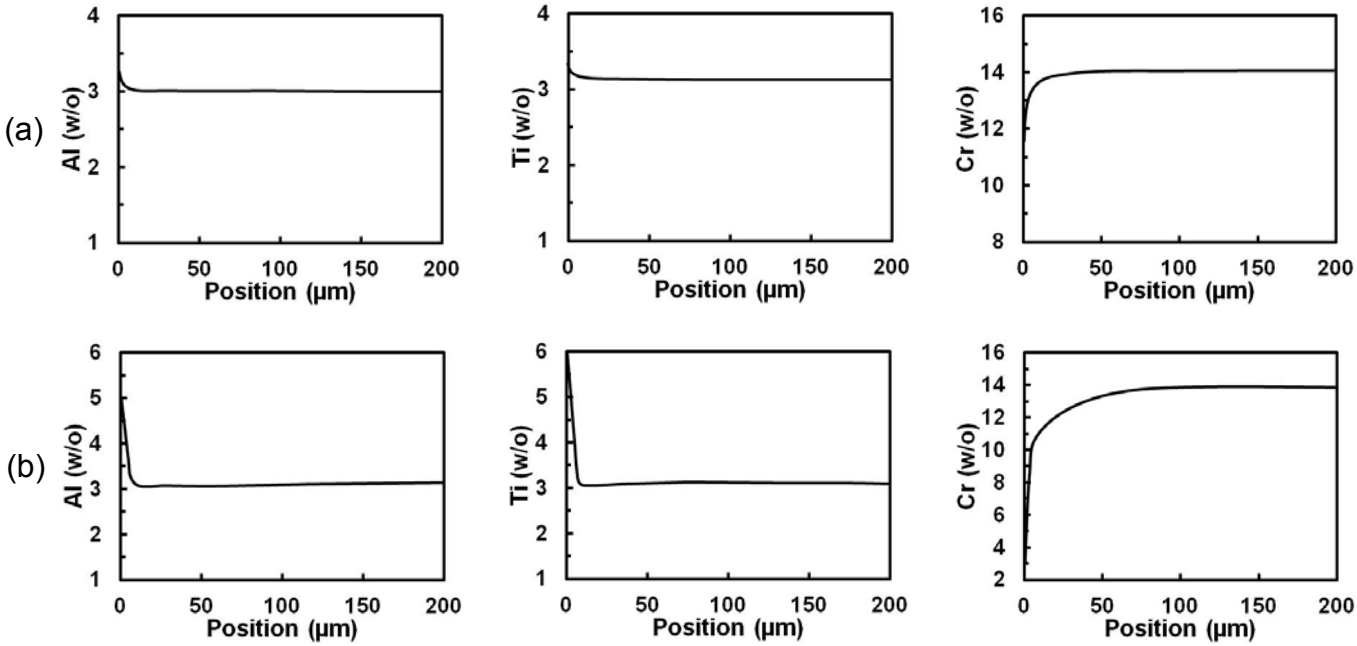

Figure 9. Concentration profiles for aluminum, titanium, and chromium as a function of distance from the free surface for LSHR samples which were heat treated in a vacuum furnace at 1408 K (1135°C) for (a) 1 h or (b) 4h.

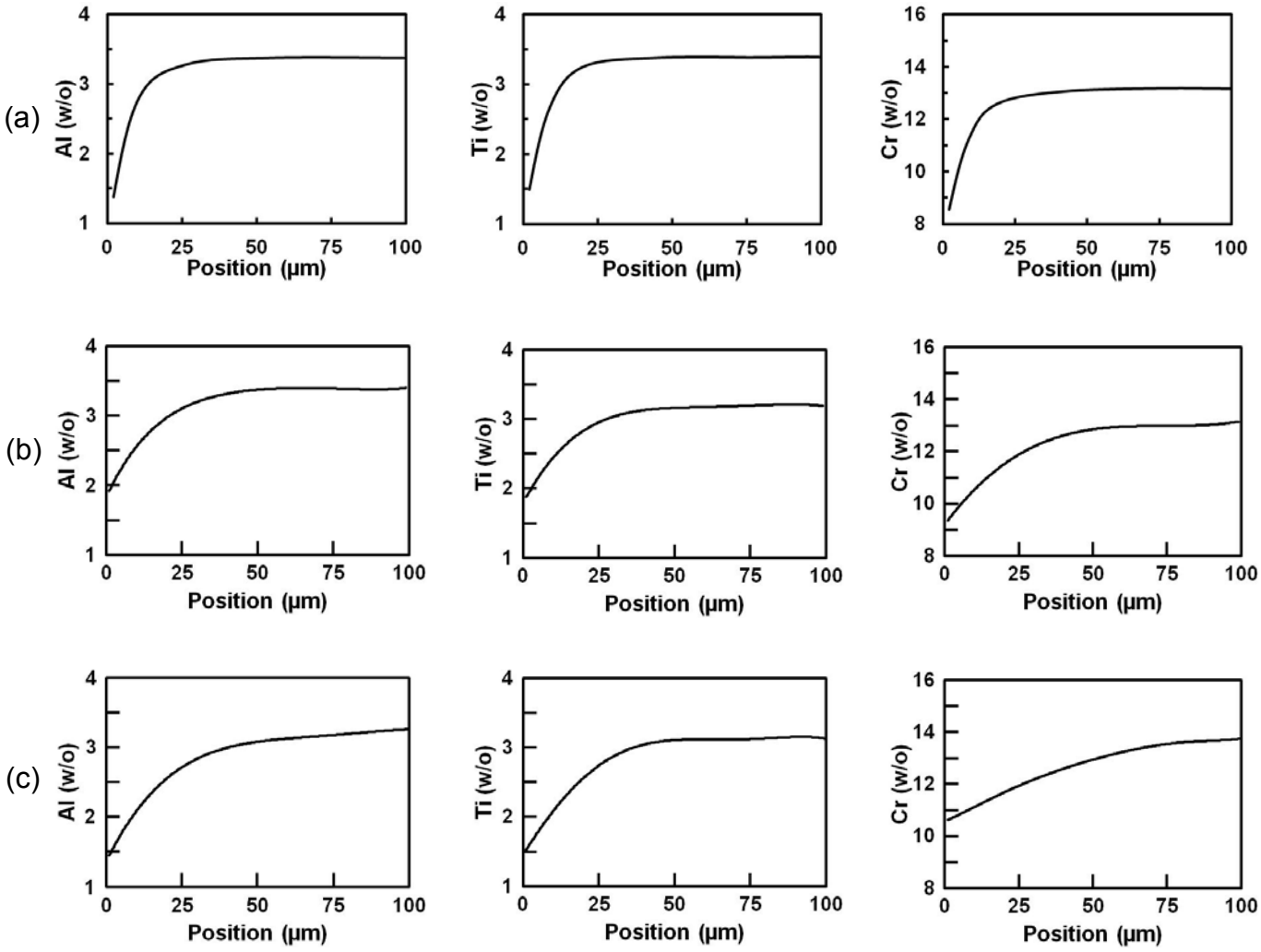

Figure 10. Concentration profiles for aluminum, titanium, and chromium as a function of distance from the metal-scale interface for LSHR samples which were heat treated without encapsulation in an air furnace at 1408 K (1135°C) for (a) 0.25 h, (b) 1 h, or (c) 4h.

May change/normalize ordinate scales to C/C_∞ to reduce scatter due to microprobe drift/errors.

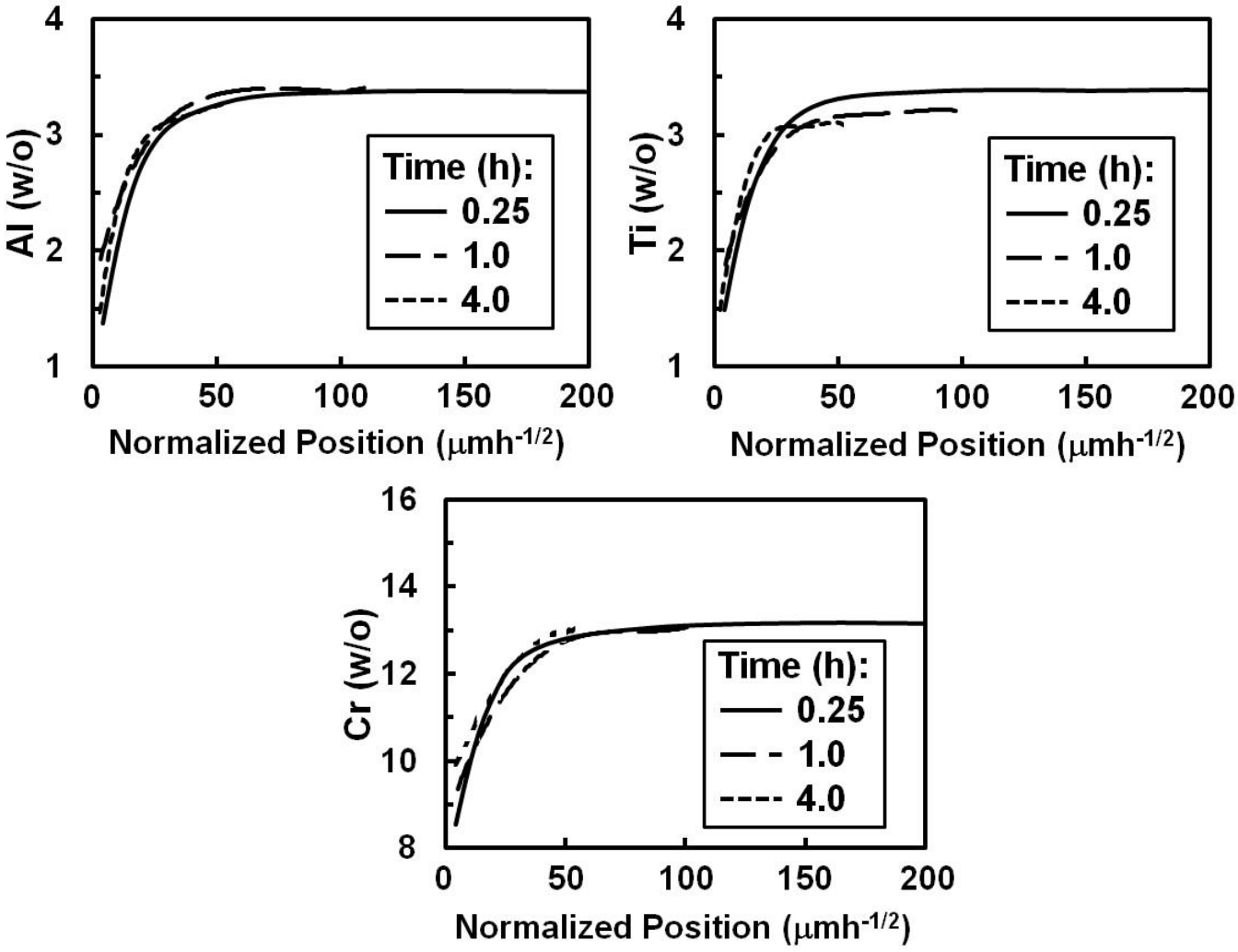

Figure 11. Concentration data for aluminum, titanium, and chromium as a function of distance from the metal-scale interface normalized by the square of exposure time for LSHR samples which were heat treated without encapsulation in an air furnace at 1408 K (1135°C).

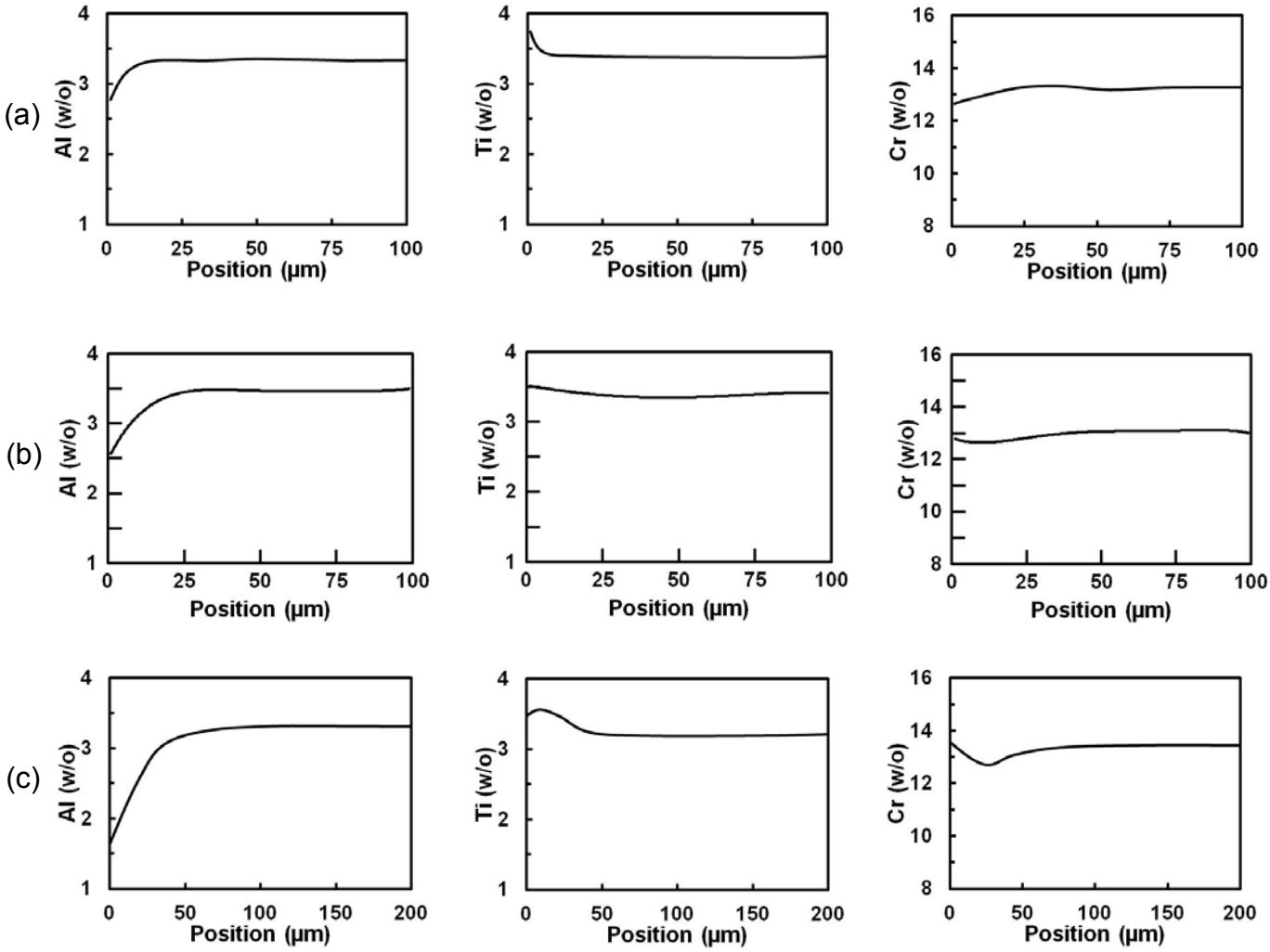

Figure 12. Concentration profiles for aluminum, titanium, and chromium as a function of distance from the free surface for LSHR samples which were heat treated in evacuated quartz capsules in an air furnace at 1408 K (1135°C) for (a) 0.25 h, (b) 1 h, or (c) 4h.

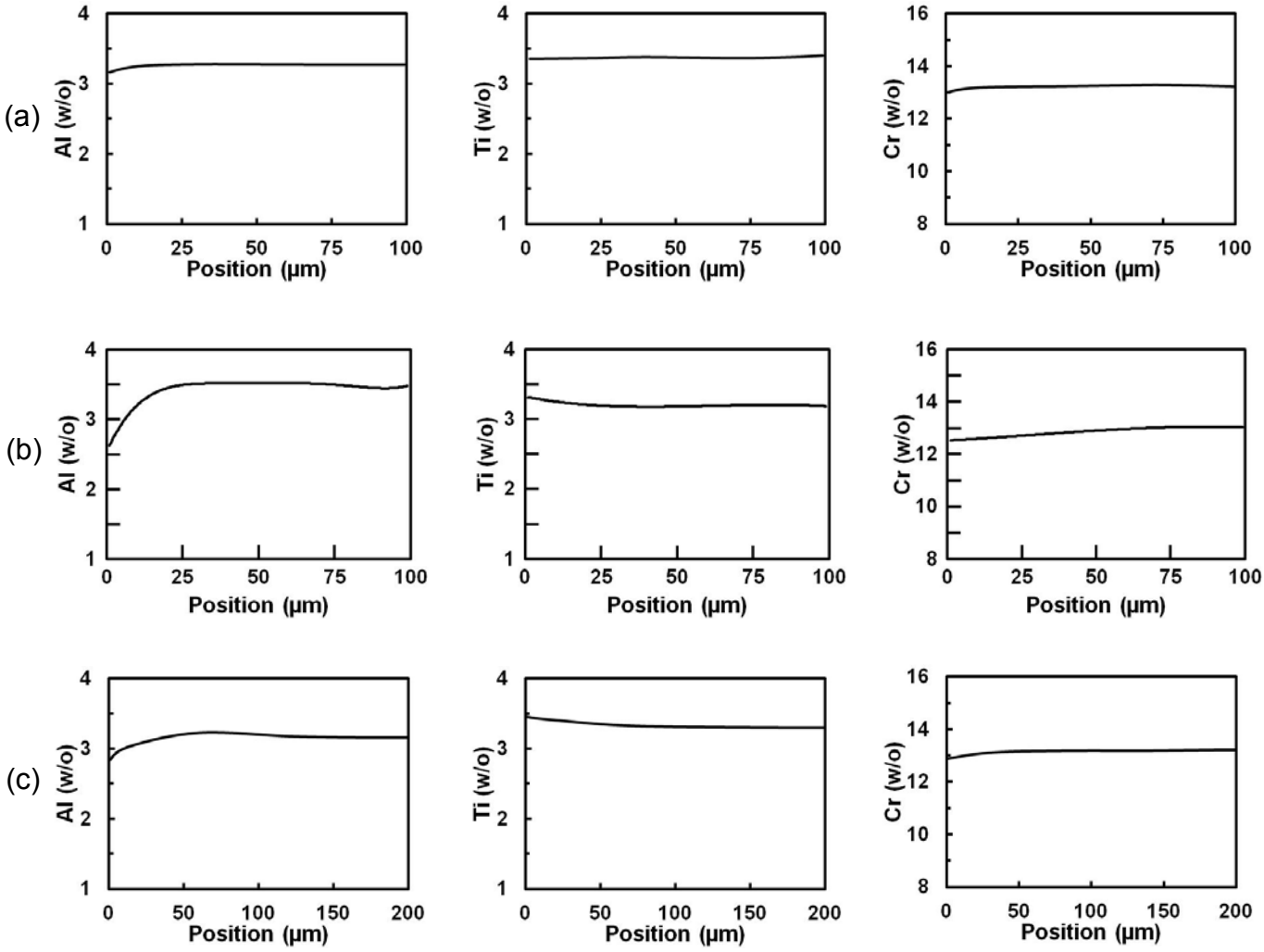

Figure 13. Concentration profiles for aluminum, titanium, and chromium as a function of distance from the free surface for LSHR samples which were heat treated in quartz capsules backfilled with argon in an air furnace at 1408 K (1135°C) for (a) 0.25 h, (b) 1 h, or (c) 4h.

May change/normalize ordinate scale to C/C_∞ to reduce scatter due to microprobe drift/errors.

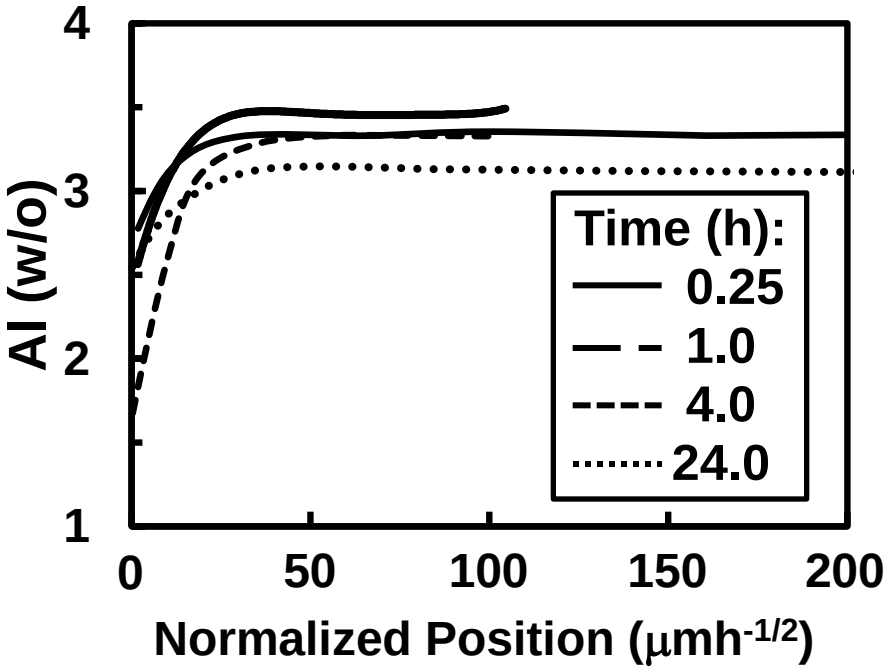

Figure 14. Concentration data for aluminum as a function of distance from the free surface normalized by the square of exposure time for LSHR samples which were heat treated in evacuated quartz capsules in an air furnace at 1408 K (1135°C).

(a)

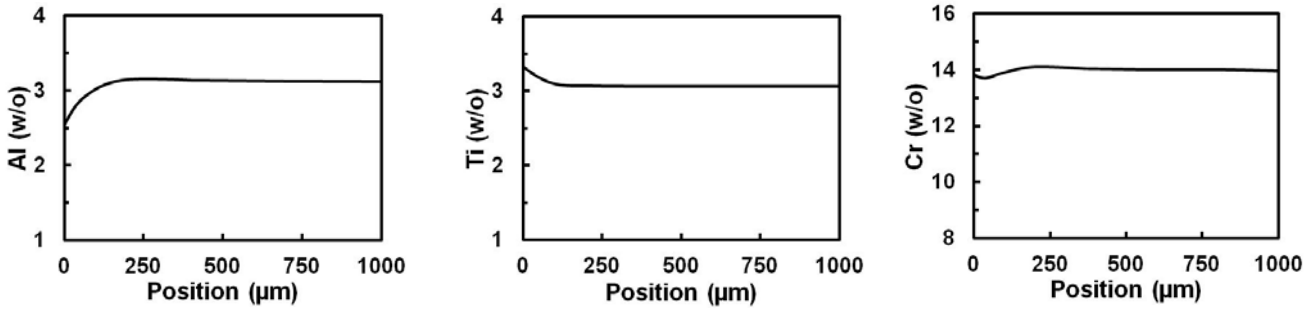

(b)

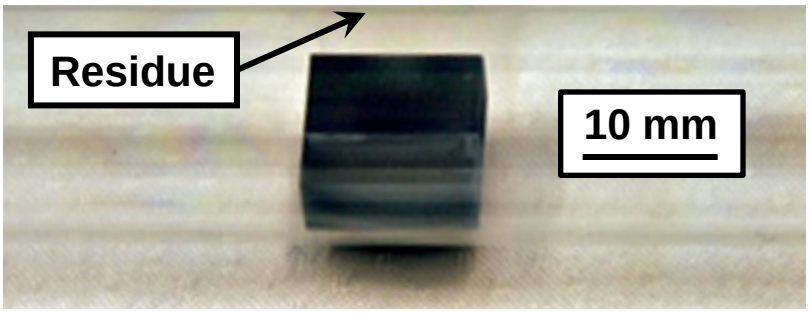

Figure 15. Observations for an LSHR sample heat treated in an evacuated quartz capsule in an air furnace at 1408 K (1135°C) for 24 h: (a) Concentration profiles for aluminum, titanium, and chromium as a function of distance from the free surface and (b) macrograph indicating discoloration of inner diameter of capsule.

(a)

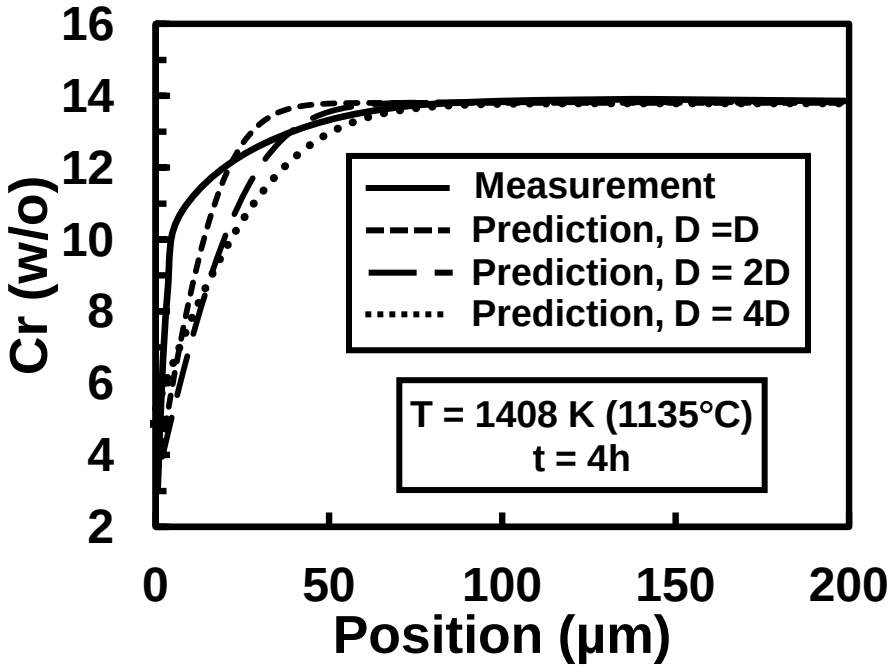

(b)

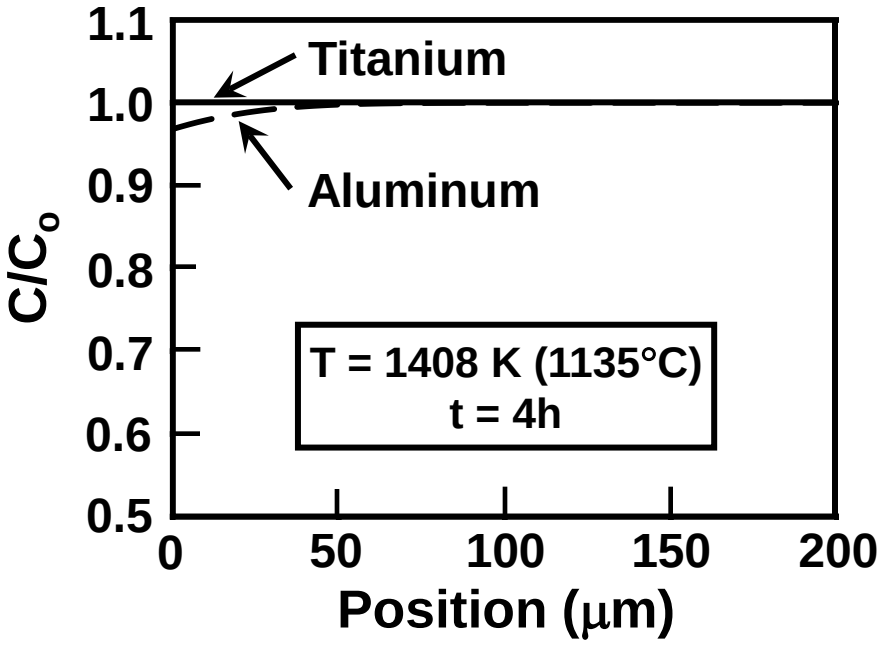

Figure 16. Evaporation model calculations for the development of concentration gradients during a 4-h heat treatment at 1408 K (1135C) in a vacuum furnace for (a) chromium or (b) aluminum and titanium.